

Giant Infrared Sensitivity of Surface Plasmon Resonance-Based Refractive Index Sensor

Akhilesh Kumar Mishra¹  · Satyendra Kumar Mishra² · Amar Pal Singh³

Received: 2 January 2017 / Accepted: 17 May 2017 / Published online: 29 May 2017
© Springer Science+Business Media New York 2017

Abstract Surface plasmons (SPs), the coherent charge density oscillations of the electrons bound to the metal-dielectric interface, are dominating the research field of optics. One of the ubiquitous applications of SPs is in sensing. In the present work, we have theoretically studied a couple of surface plasmon resonance (SPR)-based fiber-coupled ultra-sensitive refractive index sensors working in the infrared (IR) region. Either of the copper (Cu) and aluminum (Al) is used as surface plasmon exciting layers in these sensing probes. On the top of the metal layer, field-enhancing graphene and silicon layers are considered. The probes are characterized in terms of sensitivity and detection accuracy (DA). The sensitivities of Cu- and Al-based optimized probes are obtained respectively to be 23.50 and 24 $\mu\text{m}/\text{refractive index unit (RIU)}$. To ensure the probes' compatibility with bio-samples, an extra bio-recognition layer of graphene has been considered over the silicon layer which resulted into the respective sensitivities of 20 and 19.50 $\mu\text{m}/\text{RIU}$ for Cu- and Al-based probes with appreciably good DAs.

Keywords Surface plasmon · Sensitivity · Sensor · Graphene · Silicon · Fiber

✉ Akhilesh Kumar Mishra
iitd.akhilesh@gmail.com

¹ Andrew and Erna Viterbi Faculty of Electrical Engineering, Technion—Israel Institute of Technology, 32000 Haifa, Israel

² Electronic Engineering Department, City University of Hong Kong, Tat Chee Avenue, Kowloon Tong, Hong Kong

³ Faculty of Biology, Technion—Israel Institute of Technology, 32000 Haifa, Israel

Introduction

The signatory characteristic of smaller wavelength of the SPs has brought forward widespread applications encompassing imaging [1, 2], sensing [3], nano-antenna [4], metamaterials [5–7], topological insulators [8], and recently ultra-fast processing [9, 10]. Direct light lacks momentum to excite these coherent charge density oscillations and therefore extra geometrical arrangements such as high refractive index prism, optical fiber/waveguide, grating, and rough surfaces are required to fetch the direct light the requisite momentum [3]. Conventionally, noble metals are used as SP exciting metallic layer. But these metals come with their own limitations such as thin film of gold (Au) agglomerates and forms island and therefore lacks uniformity; silver (Ag) and copper (Cu), on the other hand, are chemically unstable. To circumvent these issues of noble metals, conducting metal oxides (CMOs) are usually resorted on [11, 12]. These oxides not only show good conductivity as those of noble metals but can also form very thin uniform film [13]. An alternative route of taking advantage of remarkable properties of noble metals (Ag, Cu, etc.) bypassing their chemical unstableness is to cover the metal layers with thin protecting layer of some other almost non-permeable high permittivity materials such as graphene and silicon [14]. These covering materials not only protect the underlying metal from oxidation but also enhance the field within and therefore the device performance [13, 15, 16].

One of the ubiquitous applications of SPs is in refractive index sensing [17–20]. SPs excite at the interface of metal and dielectric and its field decay evanescently in transverse directions. The evanescently decaying tail of SPs in dielectric medium is very sensitive to the complex permittivity of the dielectric material, and therefore, the phenomenon has found enormous applications in the field of refractive index sensing. To realize SP-based sensors, two configurations have been

proposed—the widely used Kretschmann configuration and the Otto configuration. Further, two methods of interrogation are practiced—wavelength interrogation and angular interrogation. Among numerous plasmonic sensing probes, optical fiber-based probes are found to demonstrate several advantageous features over other existing ones which include immunity to electromagnetic interferences, capability of remote sensing and online monitoring, miniaturization in size, ease of fabrication, and low cost.

In SP-based fiber-coupled bio-sensors, usually Au is used as SP exciting metallic layer. Au, in addition of being a chemically stable ideal (neglecting medium losses) plasmonic material, exhibits excellent bio-recognition properties. The hydrophobic surface of Au makes the immobilization of bio-entities such as proteins and antibody easy to achieve. Graphene, an sp^2 -hybridized, 2D, thinnest man-made material, has emerged as another competing plasmonic material endowed with virtues of bio-compatible materials [21]. Graphene has an extra edge on Au predominantly due to its large surface area. High charge carrier mobility incurred effective charge transfer, and the large wave vector inside the graphene results into the enhancement of the field and thereby the sensitivity of the graphene-based plasmonic sensors [22, 23]. In addition to its extensive applications in the field of sensing, it has found applications in numerous other fields such as in photo-detectors and transistors.

In the following, we propose a couple of SPR-based fiber-coupled refractive index sensors working in the IR region of the electromagnetic spectrum. As a surface exciting metallic layer, either Al or Cu has been utilized. On top of the metal layer, graphene and silicon are considered, respectively. These sensing probes are found to exhibit enormously high sensitivities with appreciable detection accuracies. Silicon being a high k -dielectric, a thin layer of it adds to the sensitivity of the device but with a limitation of formation of oxide layer on its surface which may lead to the deterioration the device performance. Furthermore, although, silicon has been reported to perform refractive index sensing, the applicability of such a probe is not promising in bio-sensing and therefore we have used graphene as an overlay which not only works as a bio-recognition layer but also protects the silicon from oxidation.

The Model

The schematic of the proposed sensing probe is shown in Fig. 1. To realize the fiber probe, cladding from the middle 1 cm section of the step-index multi-mode fiber is removed. On this bare core, a certain thickness of metal layer is deposited which is then followed by the deposition of the graphene and the silicon layers. Sensing liquid is kept in contact with the silicon layer. Transverse magnetically (TM) polarized light, from a polychromatic source, is launched in one end of the

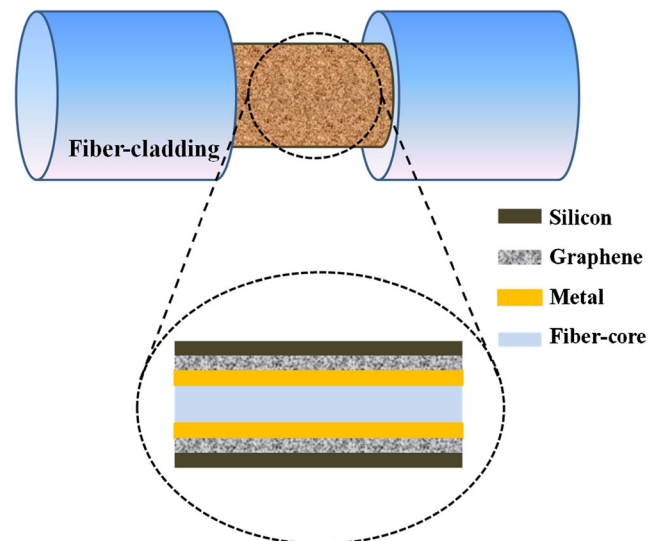


Fig. 1 Schematic of the fiber probe

fiber and the transmitted light is detected from the other end. Light guiding in the fiber, on phase matching, gets coupled resonantly to the surface mode (SP). This phenomenon of resonant energy transfer is termed as surface plasmon resonance (SPR). The phase matching criteria for resonant transfer of energy is met at a particular wavelength, known as resonance wavelength λ_{res} . The loss of the guided light due to the out-coupling appears at the output as a dip in the transmission/SPR spectrum.

These sensors are usually characterized in terms of sensitivity and detection accuracy (DA) which are defined respectively as

$$\text{Sensitivity} = \frac{\Delta\lambda_{res}}{\Delta n_s}; \quad (1)$$

where numerator represents a change in resonance wavelength and the denominator the corresponding change in the refractive index of the sensing medium (n_s);

$$DA = \frac{1}{\Delta\lambda_{fwhm}}; \quad (2)$$

where denominator represents the full width at half maximum of the resonance dip. DA predicts the accuracy with which minimum of the resonance dip can be located.

The position of the dip in the transmission spectrum varies with the sensing medium refractive index (RI). In the proposed study, we have chosen the RI of the sensing medium $n_s = 1.330$ RIU and the change in the RI introduced by the adsorption of bio-molecules $\Delta n_s = 0.002$ RIU. Choosing aqueous sensing medium RI equal to 1.330 RIU has wide open prospects in bio-sensing as the ambient RI environment of most of the bio-samples is around 1.330 RIU. For simulation, the diameter of the fiber is taken to be 600 μm and the numerical aperture 0.24.

Table 1 Dispersion coefficients for metals

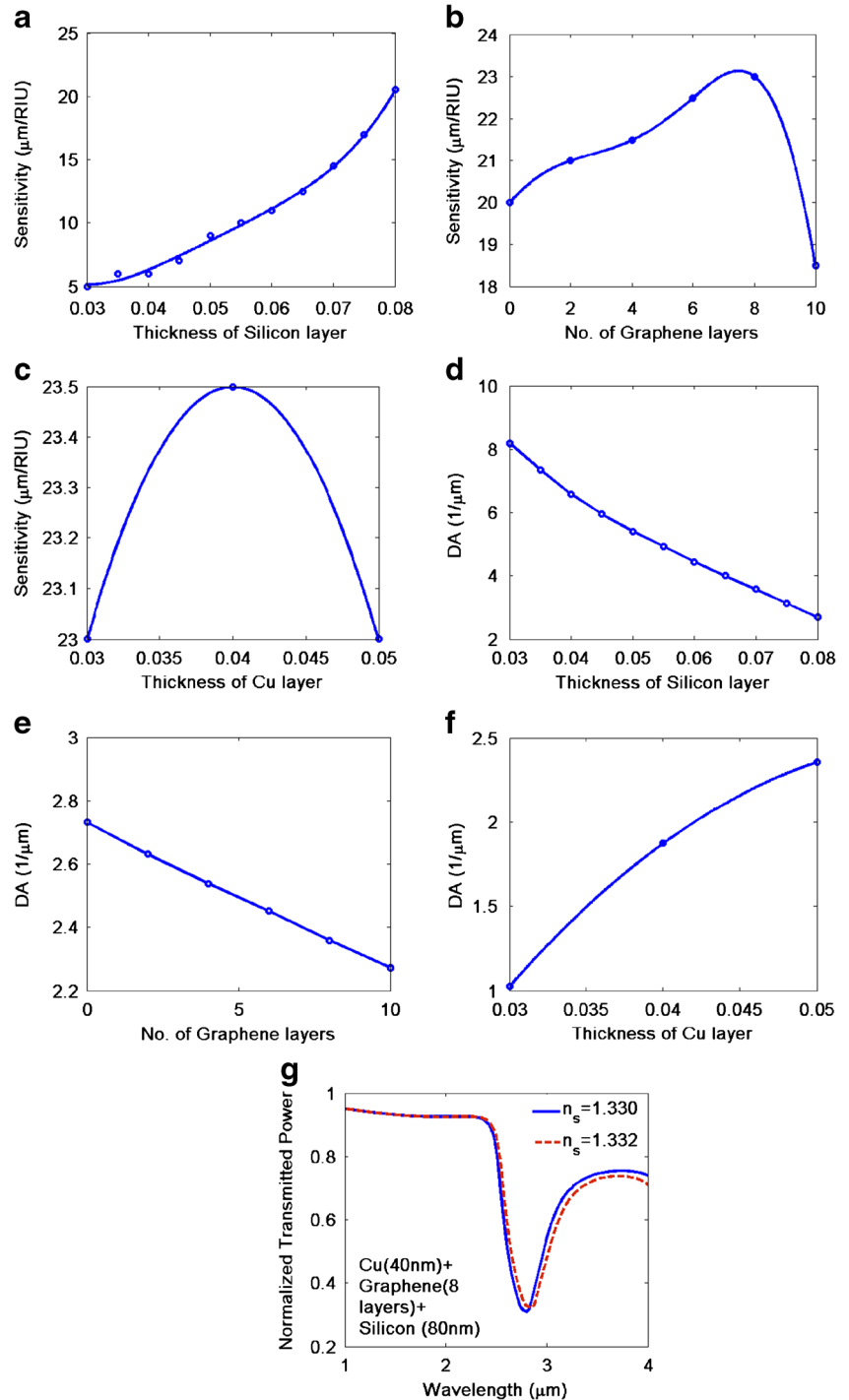
Dispersion coefficients (μm)	Metals [14]	
	Cu	Al
λ_p	0.13617	0.10657
λ_c	40.852	24.511

Dispersion Relations

For dispersive modeling of the different materials involved, following dispersion relations have been used:

Dispersive behavior of the RI of the fiber core material is accounted for by Sellmeier relation given as [14]

Fig. 2 **a** Variation of sensitivity with thickness (in μm) of silicon layer for probe with 50 nm of Cu layer and single layer of graphene. **b** Variation of sensitivity with number of graphene layers for probe with 50 nm of Cu layer and 80 nm of silicon layer. **c** Variation of sensitivity with thickness (in μm) of Cu layer for probe with eight layers of graphene and 80 nm of silicon layer. **d** Variation of DA with thickness (in μm) of silicon layer for probe with 50 nm of Cu layer and single layer of graphene. **e** Variation of DA with number of graphene layers for probe with 50 nm of Cu layer and 80 nm of silicon layer. **f** Variation of DA with thickness (in μm) of Cu layer for probe with eight layers of graphene and 80 nm of silicon layer. **g** SPR (transmission) curves for probe with 40 nm of Cu layer, eight layers of graphene, and 80 nm silicon layer. n_s represents the refractive index of the sensing layer



$$n_{\text{core}}(\lambda) = \sqrt{1 + \frac{a_1\lambda^2}{\lambda^2 - b_1^2} + \frac{a_2\lambda^2}{\lambda^2 - b_2^2} + \frac{a_3\lambda^2}{\lambda^2 - b_3^2}}; \tag{3}$$

where a_s and b_s are the Sellmeier coefficients and for pure silica glass

$$a_1 = 0.6961663, \quad a_2 = 0.4079426, \quad a_3 = 0.8974794, \\ b_1 = 0.0684043, \quad b_2 = 0.1162414, \quad b_3 = 9.896161$$

Drude relation is used to model the wavelength dispersion of metals [14]

$$\varepsilon(\lambda) = \varepsilon_r + i\varepsilon_i = 1 - \frac{\lambda^2\lambda_c}{\lambda_p^2(\lambda_c + i\lambda)}; \tag{4}$$

where λ_p is the wavelength corresponding to the bulk plasma frequency and λ_c denotes the collision wavelength and is related to the medium losses. The values of λ_p and λ_c for Cu and Al are listed in Table 1.

The dispersion relation of the graphene reads as [24, 25]

$$n(\lambda) = 3.0 + i\frac{C}{3}\lambda; \tag{5}$$

where $C = 5.446/\mu\text{m}$ is a constant. The single sheet thickness of graphene is ~ 0.34 nm. Its total thickness depends on the total number of deposited layers (\mathcal{L}) and is given as $0.34 * \mathcal{L}$ nm.

Dispersive modeling of the silicon is accomplished using the following relation [26]

$$n = A + A_1e^{-\lambda/t_1} + A_2e^{-\lambda/t_2}; \tag{6}$$

where $A = 3.44904$, $A_1 = 2271.88813$, $A_2 = 3.39538$, $t_1 = 0.05304$, and $t_2 = 0.30384$. The wavelength (λ) in all of the above relations is measured in micron.

Transmitted Power Calculation

Out of all the rays launched into the fiber input face, only those gets guided which are launched within a well-defined range of angle varying from $\theta_1 = \sin^{-1}(n_{cl}/n_{core})$ to $\theta_2 = \pi/2$, where n_{core} and n_{cl} are, respectively, the refractive indices of the fiber core and the cladding. The angle θ is the angle between the ray and the normal to the core-cladding interface of the fiber. The total transmitted power delivered at the output end of the fiber, considering the guidance of all the launched rays, is given by [13]

$$P_{\text{trans}} = \frac{\int_{\theta_1}^{\theta_2} R_p^{N_{\text{ref}}(\theta)} \frac{n_{\text{core}}^2 \sin\theta \cos\theta}{(1 - n_{\text{core}}^2 \cos^2\theta)^2} d\theta}{\int_{\theta_1}^{\theta_2} \frac{n_{\text{core}}^2 \sin\theta \cos\theta}{(1 - n_{\text{core}}^2 \cos^2\theta)^2} d\theta} \tag{7}$$

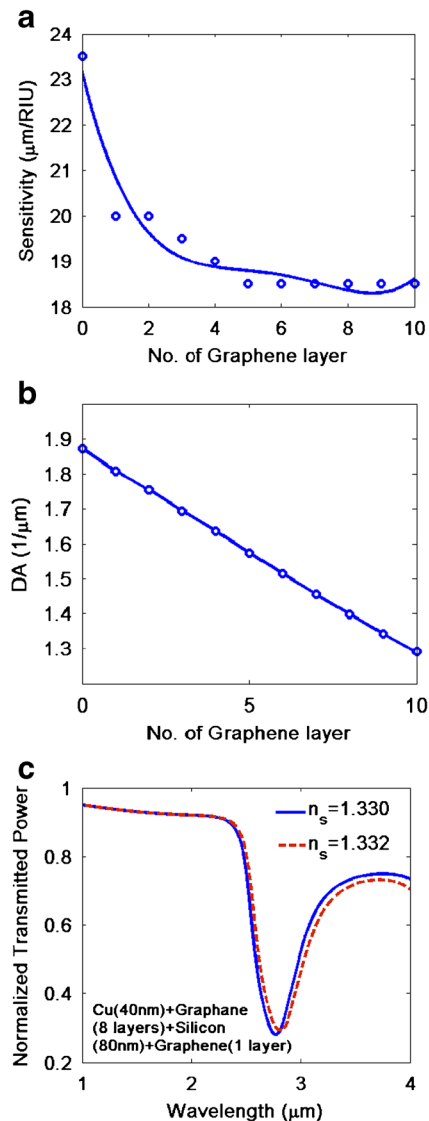


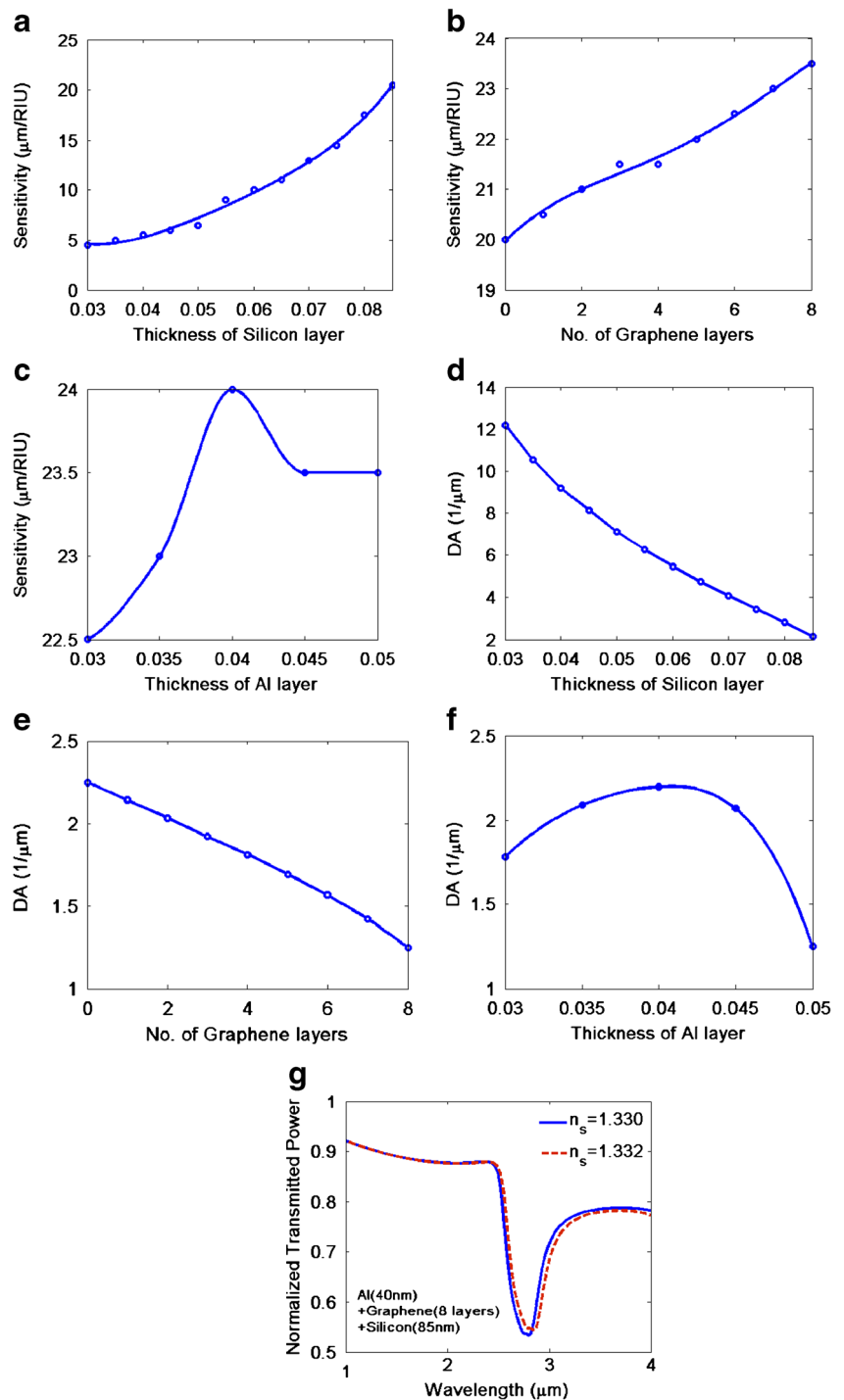
Fig. 3 a Variation of sensitivity with number of outer graphene layers for probe with 40 nm of Cu layer, eight layers of inner graphene, and 80 nm of silicon layer. b Variation of DA with number of outer graphene layers for probe with 40 nm of Cu layer, eight layers of inner graphene, and 80 nm of silicon layer. c SPR (transmission) curves for probe with 40 nm of Cu layer, eight layers of inner graphene, 80 nm silicon layer, and single layer of outer graphene. n_s represents the refractive index of the sensing layer

Where $N_{\text{ref}}(\theta) = \frac{L}{D \tan\theta}$; $N_{\text{ref}}(\theta)$ is the total number of reflections undergone by the ray in sensing probe of length L and core diameter D . R_p is reflectance calculated using Fresnel’s formulae and well-developed multi-layer matrix method [27, 28].

Results and Discussion

In the following, we have studied the two SPR-based fiber-coupled sensors: the first using Cu as metal layer and the second using Al as metal layer. These two sensors are characterized in

Fig. 4 **a** Variation of sensitivity with thickness (in μm) of silicon layer for probe with 50 nm of Al layer and single layer of graphene. **b** Variation of sensitivity with number of graphene layers for probe with 50 nm of Al layer and 85 nm of silicon layer. **c** Variation of sensitivity with thickness (in μm) of Al layer for probe with eight layers of graphene and 85 nm of silicon layer. **d** Variation of DA with thickness (in μm) of silicon layer for probe with 50 nm of Al layer and single layer of graphene. **e** Variation of DA with number of graphene layers for probe with 50 nm of Al layer and 85 nm of silicon layer. **f** Variation of DA with thickness (in μm) of Al layer for probe with eight layers of graphene and 85 nm of silicon layer. **g** SPR (transmission) curves for probe with 40 nm of Al layer, eight layers of graphene, and 85 nm silicon layer. n_s represents the refractive index of the sensing layer



terms of sensitivity and DA. All the characterizations have been performed such that the transmission dips always be confined within the wavelength stretch of 1 to 3 μm which is well in the infrared region of the electromagnetic spectrum. Also, we have assumed that the abovementioned dispersion relations for the different layers are valid in the wavelength window of investigation. During optimization of the probe for sensitivity, it has been taken care of that DA always remains definable, i.e., arms of the

transmission dips do not become shallower than the half of the maximum of the transmitted power (see ref. [14]). The details of the two probes are as follows.

Probe Using Cu as Metal Layer

To realize the probe, Cu is considered over the unclad portion of the fiber core which is followed by the graphene layers and

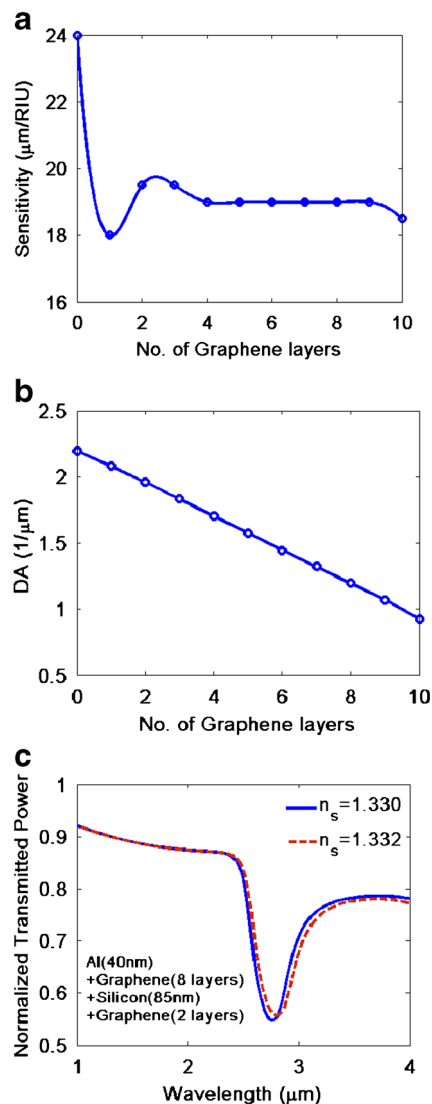


Fig. 5 **a** Variation of sensitivity with number of outer graphene layers for probe with 40 nm of Al layer, eight layers of inner graphene, and 85 nm of silicon layer. **b** Variation of DA with number of outer graphene layers for probe with 40 nm of Al layer, eight layers of inner graphene, and 85 nm of silicon layer. **c** SPR (transmission) curves for probe with 40 nm of Al layer, eight layers of inner graphene, 85 nm silicon layer, and two layers of outer graphene. n_s represents the refractive index of the sensing layer

then silicon as shown in Fig. 1. To start with, thickness of the Cu layer is fixed at 50 nm and only single sheet of graphene (single sheet thickness $\mathcal{L} \sim 0.34$ nm) is considered. The thickness of the upper most layer of silicon is varied to maximize the sensitivity of the probe. Figure 2a shows the variation of sensitivity of this probe with thickness of silicon layer. The figure clearly depicts that with increasing thickness of silicon the sensitivity of the probe increases. We restricted the increasing thickness of silicon at 80 nm because beyond this thickness the transmission dip crosses the far edge (3 μm) of our wavelength window of investigation. Note that in Fig. 2a and in the figures thereafter,

the layer thicknesses (on x -axis) are in the unit of micron. Next to optimize the no. of graphene layers, we fix the Cu layer thickness at 50 nm and silicon layer thickness at its optimized value of 80 nm. Figure 2b shows the variation of sensitivity with no. of graphene layers, and it can be observed that sensitivity becomes maximum for eight layers of graphene and therefore $8 * \mathcal{L}$ is the optimized thickness of the graphene layer. Note that with the addition of the graphene sheets, the sensitivity increases up to a certain limit and thereafter it starts to decrease. This behavior is attributed to the fact that at higher thickness of graphene, the losses of graphene sheets take over and therefore the electric field and hence the sensitivity enhancing characteristic of graphene deteriorate. Variation of sensitivity with Cu layer thickness is shown in Fig. 2c for probe with eight layers of graphene and 80 nm of silicon layer thickness. Maximum sensitivity of 23.50 $\mu\text{m}/\text{RIU}$ is observed for probe with 40 nm thickness of Cu layer. Figure 2d–f reveals the corresponding cases of variation of DAs with different layers' thicknesses as depicted in Fig. 2a–c, respectively. DA for the probe optimized for maximum sensitivity is found to be 1.879/ μm . The SPR (transmission) spectra at the two values of the sensing medium RI for the optimized probe are presented in Fig. 2g which clearly shows that the SPR dips are well below the 3 μm wavelength limit.

Further, to make the above probe compatible with the bio-sample sensing, either the silicon's surface is to be activated with proper antigen, enzymes, etc. or a thin layer of bio-adsorbing material is to be coated on it. Owing to the excellent bio-adsorbing characteristics of graphene, we consider a few sheets of graphene on the previously optimized probe. As shown in Fig. 3a, with the deposition of graphene sheets, the sensitivity of the device decreases. As a trade-off, we choose only single sheet of graphene. This optimized probe results a maximum sensitivity of 20 $\mu\text{m}/\text{RIU}$ with DA of 1.808/ μm (Fig. 3b). Decrease in the DA with graphene layer thickness in Fig. 3b also reveals the lossy nature of the graphene sheet. Figure 3c shows the corresponding SPR spectra.

Probe Using Al as Metal Layer

In this probe design, the Cu layer in the previous probe is replaced with Al leaving the rest of the layers the same. Initially, the thickness of Al is fixed at 50 nm, single layer of graphene is considered, and the thickness of silicon layer is varied to maximize the sensitivity of the probe as shown in Fig. 4a. As we increase the thickness of silicon layer, sensitivity increases but as soon as the thickness goes beyond to 85 nm, the DA becomes undefined (due to the shallowness of longer wavelength arm of the dip) and alongside the SPR dip crosses the 3 μm limit. Hence, we choose 85 nm as optimized thickness of the silicon layer.

Table 2 Summary of results

Parameters	Probes			
	Cu (40 nm)/graphene (8 layers)/silicon (80 nm)	Cu (40 nm)/graphene (8 layers)/silicon (80 nm)/graphene (1 layer)	Al (40 nm)/graphene (8 layers)/silicon (85 nm)	Al (40 nm)/graphene (8 layers)/silicon (85 nm)/graphene (2 layers)
Sensitivity ($\mu\text{m}/\text{RIU}$)	23.5	20.0	24.0	19.5
Detection accuracy ($/\mu\text{m}$)	1.879	1.808	2.198	1.961

In Fig. 4b, the no. of graphene sheets are optimized for maximum sensitivity of the probe with 50 nm of Al layer and optimized 85 nm thickness of silicon. The sensitivity is maximum for eight layers of graphene and beyond this no. of graphene layers the DA becomes undefined. In Fig. 4c, we have optimized the thickness of Al layer which comes out to be 40 nm with sensitivity of 24 $\mu\text{m}/\text{RIU}$. Figure 4d–f shows the corresponding DAs. DA for the optimized design is found to be 2.198/ μm . The SPR plots for such a probe are shown in Fig. 4g.

Now, as discussed previously, for bio-sensing purposes, we consider a bio-recognition graphene layer on the top of the silicon layer. To optimize the no. of graphene layers, the sensitivity of this modified probe is observed with respect to the no. of graphene layers as depicted in Fig. 5a. The sensitivity is maximum (19.50 $\mu\text{m}/\text{RIU}$) when no. of graphene layers are either two or three. We choose two layers of graphene for our optimized design to have better DA which is 1.961/ μm as shown in Fig. 5b. SPR plots for this probe showing SPR activity in the IR region are depicted in Fig. 5c.

As a concise summary, all the results of the present study are listed in Table 2. Note that the metals used in the study are highly chemically reactive and easily forms oxides. But, since they are protected with overlays of graphene and silicon, their chemical instability is no more an issue. Further, use of Cu and

Al, being low-cost materials as compared to the Au and Ag, reduces the overall cost of the sensing probe considerably. The optimum value of sensitivity complying with the constraint of DA (i.e., definable fwhm width of transmission minima) resulted out of this study is 24 $\mu\text{m}/\text{RIU}$ which, to the widest of our knowledge, is highest in the IR region around the given aqueous sensing medium RI range (see Table 3). Additionally, the sensitivity could further be increased by increasing the sensing medium refractive index until it becomes almost equal to that of the fiber core.

Table 3 presents a comprehensive comparative study of the proposed and the other exiting SPR-based sensing probes working in the IR domain of electromagnetic spectrum with sensing medium RI varying around that of water. The only comparable sensitivity is reported in ref. [32], but the SPR curves therein do not satisfy the constraint set by our definition of DA, i.e., DA is extremely poor and therefore proposed sensors stand far better.

Conclusion

A couple of SPR-based fiber-coupled IR sensors have been studied. Constituent layers of the probes are optimized, under

Table 3 Comparison with SPR-based IR sensors

Sensor type	Refractive index range (RIU)	Wavelength window of operation (μm)	Sensitivity ($\mu\text{m}/\text{RIU}$)	Note	Reference
D shape PCF	1.33–1.37	1.40–2.10	5.2	–	[29]
Fiber sensor with tilted FBG	1.33–1.37	1.10–1.70	18	Sensitivity is high only for higher RI (around 1.36 RIU)	[30]
Fiber sensor	1.20–1.21	1.0–2.2	3.125	–	[31]
Fiber sensor	1.332–1.336	0.50–0.95	24 \pm 3	Extremely poor experimental DA	[32]
Waveguide couple fiber sensor	1.332–1.38	0.4–1.1	2.017	–	[33]
Fiber sensor	1.33–1.37	1.2–3.0	15.07	Sensitivity is high only for higher RI (around 1.36 RIU)	[15]
Fiber sensor	1.330–1.332	0.4–1.0	6.2	–	[14]
Grazing angle incidence on a planner substrate	1.33–1.47	1.37–2.49	8.3	Sensitivity is high only for higher RI (>1.39 RIU)	[34]
Fiber sensor	1.330–1.332	1.0–3.0	24	–	Present study

the constraint set by DA, to exhibit giant sensitivities of 23.50 and 24 $\mu\text{m}/\text{RIU}$ for probes using Cu and Al as metallic layer, respectively. The optimized design parameters of the probes are Cu (40 nm)/graphene (eight layers)/silicon (80 nm) and Al (40 nm)/graphene (eight layers)/silicon (85 nm). The corresponding bio-sensors having additional layers of graphene (single and two layers respectively) exhibit sensitivities of 20 and 19.50 $\mu\text{m}/\text{RIU}$ with appreciably good DAs.

We hope that the present study will have high impact in bio- and chemical sensing.

Acknowledgements Akhilesh Kumar Mishra acknowledges the support in part at Technion by Israel Council for Higher Education.

References

- Nicoletti O, de la Pena F, Leary RK, Holland DJ, Ducati C, Midgley PA (2013) Three-dimensional imaging of localized surface plasmon resonances of metal nanoparticles. *Nature* 502:80–84
- Gong Y, Joly AG, Hu D, El-Khoury PZ, Hess WP (2015) Ultrafast imaging of surface plasmons propagating on a gold surface. *Nano Lett* 15:3472–3478
- Homola J (2006) Surface plasmon resonance based sensors, Springer Series on Chemical Sensors and Biosensors. Vol. 4. Springer, Berlin
- Mühschlegel P, Eisler H-J, Martin OJF, Hecht B, Pohl DW (2005) Resonant optical antennas. *Science* 308:1607–1609
- Lezec HJ, Dionne JA, Atwater HA (2007) Negative refraction at visible frequencies. *Science* 316:430–432
- Kumar A, Mishra AK (2012) Anomalous self-steepening, temporal pulse splitting and ring formation in a left-handed metamaterial with cubic nonlinearity. *J Opt Soc Am B* 29:1330–1337
- Mishra AK, Kumar A (2012) Novel high gain regimes of spatio-temporal modulational instability for a single-cycle pulse in metamaterials. *J Mod Opt* 59:1599–1606
- Politano A, Silkin VM, Nechaev IA, Vitiello MS, Viti L, Aliev ZS, Babanly M B, Chiarello G, Echenique P M, Chulkov EV (2015) Interplay of surface and Dirac plasmons in topological insulators: the case of Bi_2Se_3 . *Phys Rev Lett* 115:216802
- Lereu AL (2007) Modulation: plasmons lend a helping hand. *Nat Photonics* 1:368–369
- Wurtz GA, Pollard R, Hendren W, Wiederrecht GP, Gosztola DJ, Podolskiy VA, Zayats AV (2011) Designed ultrafast optical nonlinearity in a plasmonic nanorod metamaterial enhanced by nonlocality. *Nat Nanotechnol* 6:107–111
- Rhodes C, Franzen S, Maria J-P, Losego M, Leonard DN, Laughlin B, Duscher G, Weibel S (2006) Surface plasmon resonance in conducting metal oxides. *J Appl Phys* 100:054905
- Franzen S, Rhodes C, Cerruti M, Gerber RW, Losego M, Maria J-P, Aspnes DE (2009) Plasmonic phenomena in indium tin oxide and ITO-Au hybrid films. *Opt Lett* 34:2867–2869
- Mishra AK, Mishra SK, Gupta BD (2015) SPR based fiber optic sensor for refractive index sensing with enhanced detection accuracy and figure of merit in visible region. *Opt Commun* 344:86–91
- Mishra AK, Mishra SK, Verma RK (2016) Graphene and beyond graphene MoS_2 : a new window in surface-plasmon-resonance-based fiber optic sensing. *J Phys Chem C* 120:2893–2900
- Mishra AK, Mishra SK (2015) Infrared SPR sensitivity enhancement using ITO/ TiO_2 /silicon overlayers. *Europhys Lett* 112:10001
- Shalabney A, Abdulhalim I (2010) Electromagnetic fields distribution in multilayer thin film structures and the origin of sensitivity enhancement in surface plasmon resonance sensors. *Sensors Actuators A Phys* 159:24–32
- Nishijima Y, Rosa L, Juodkazis S (2014) Long-range interaction of localized surface plasmons in periodic and random patterns of Au nanoparticles. *Appl Phys A* 115:409–414
- Mishra AK, Mishra SK, Verma RK (2015) An SPR-based sensor with an extremely large dynamic range of refractive index measurements in the visible region. *J Phys D Appl Phys* 48:435502
- Mishra AK, Mishra SK, Gupta BD (2015) Gas-clad two-way fiber optic SPR sensor: a novel approach for refractive index sensing. *Plasmonics* 10:1071–1076
- Nishijima Y, Adachi Y, Rosa L, Juodkazis S (2013) Augmented sensitivity of an IR-absorption gas sensor employing a metal hole array. *Opt Mat Exp* 3:968–976
- Kuila T, Bose S, Khanra P, Mishra AK, Kim NH, Lee JH (2011) Recent advances in graphene-based biosensors. *Biosens Bioelectron* 26:4637–4648
- Wu L, Chu HS, Koh WS, Li EP (2010) Highly sensitive graphene biosensors based on surface plasmon resonance. *Opt Exp* 18:14395–14400
- Mishra AK, Mishra SK (2017) MgF₂ prism/rhodium/graphene: efficient refractive index sensing structure in optical domain. *J Phys Condens Matter* 29:145001
- Bruna M, Borini S (2009) Optical constants of graphene layers in the visible range. *Appl Phys Lett* 94:031901
- Nair RR, Blake P, Grigorenko AN, Novoselov KS, Booth TJ, Stauber T, Peres NMR, Geim AK (2008) Fine structure constant defines visual transparency of Graphene. *Science* 320:1308–1308
- Mishra AK, Mishra SK (2016) Gas sensing in Kretschmann configuration utilizing bi-metallic layer of Rhodium-Silver in visible region. *Sensors Actuators B Chem* 237:969–973
- Hansen WN (1968) Electric fields produced by the propagation of plane coherent electromagnetic radiation in a stratified medium. *J Opt Soc Am* 58:380–390
- Chilwell J, Hodgkinson I (1984) Thin-films field-transfer matrix theory of planar multilayer waveguides and reflection from prism-loaded waveguides. *J Opt Soc Am A* 1:742–753
- Dash JN, Jha R (2016) Highly sensitive D shaped PCF sensor based on SPR for near IR. *Opt Quant Electron* 48:137
- Allsop T, Neal R, Rehman S, Webb DJ, Mapps D, Bennion I (2008) Characterization of infrared surface plasmon resonances generated from a fiber-optical sensor utilizing tilted Bragg gratings. *J Opt Soc Am B* 25:481–490
- Verma RK, Gupta BD (2010) Surface plasmon resonance based fiber optic sensor for the IR region using a conducting metal oxide film. *J Opt Soc Am A* 27:846–851
- Masson J-F, Kim Y-C, Obando LA, Peng W, Booksh AS (2006) Fiber-optic surface plasmon resonance sensors in the near-infrared spectral region. *Appl Spectrosc* 60:1241–1246
- Ahn JH, Seong TY, Kim WM, Lee TS, Kim I, Lee K-S (2012) Fiber-optic waveguide coupled surface plasmon resonance sensor. *Opt Exp* 20:21729–21738
- Torres V, Beruete M, Sánchez P, Villar ID (2016) Indium tin oxide refractometer in the visible and near infrared via lossy mode and surface plasmon resonances with Kretschmann configuration. *Appl Phys Lett* 108:043507